Chula Med J Vol. 68 No. 3 July - September 2024; 203 - 218 DOI : 10.56808/2673-060X.5424

Original article

Identification and characterization of malaria box compounds possessing inhibition effect on the SARS-CoV-2 spike protein

Chotiyapat Sangvansindhu[a], Pakaporn Patchimnan[a], Yaowaluck Maprang Roshorm[b], Anchanee Kubera[a, *]

[a]*Department of Genetics, Faculty of Science, Kasetsart University, Bangkok, Thailand*

[b]*Division of Biotechnology, School of Bioresources and Technology, King Mongkut's University Thonburi, Bangkok, Thailand*

Abstract

Background: The severe acute respiratory syndrome coronavirus 2 (SARS-CoV-2) has caused millions of infections and deaths worldwide since 2019. Although current treatments are available for patients with mild-to-moderate symptoms, they have limited efficacy in severe COVID-19 and can cause side effects in some patient groups, particularly in older or nonhealthy individuals. Developing new drugs that can better manage severe disease, reduce mortality rates, and broaden the treatment options are necessary.
Objective: To evaluate the binding interactions and inhibitory effect of malaria box compounds on the B-cell epitope regions of SARS-CoV-2 spike protein.
Methods: Molecular docking of 400 malaria box compounds against the predicted B-cell epitopes of the spike protein was performed. The inhibitory effects of malaria box compounds on the spike RBD were determined using competitive enzyme-linked immunoassay. The binding affinity between malaria box compounds and non-RBD epitopes was examined by surface plasmon resonance (SPR) assays.
Results: MMV000563 and MMV019690 were the top-scoring compounds that could bind to the spike RBD, with inhibitory effects at 45.6% and 47.0%, respectively. However, competitive ELISA revealed that the binding of the spike RBD to human angiotensin-converting enzyme 2 was most strongly inhibited by MMV665881 ($P = 0.004$). Based on SPR results, MMV019881, MMV020912, and MMV000753 showed the highest binding affinities to their respective epitope peptides in the non-RBD regions of the spike protein.
Conclusion: These results demonstrate the ability of malaria box compounds to bind to and interfere with SARS-CoV-2 spike protein, which may be beneficial for COVID-19 treatment.

Keywords: B-cell epitope, malaria box, molecular docking, SARS-CoV-2, spike protein.

Severe acute respiratory syndrome coronavirus 2 (SARS-CoV-2) is a novel coronavirus that is responsible for the coronavirus disease 2019 (COVID-19) pandemic starting in late 2019.(1) Within 3 years, at least 12 SARS-CoV-2 variants had been identified.(2) With its high infection rate, long incubation period, and rapid mutation rate, the virus has spread to more than 213 countries and territories worldwide, with more than 689 million confirmed cases and 6.9 million deaths thus far.(1)

***Correspondence to: Anchanee Kubera**, Department of Genetics, Faculty of Science, Kasetsart University, Bangkok 10900, Thailand.
E-mail: fsciacs@ku.ac.th
Received: March 4, 2024
Revised: May 14, 2024
Accepted: June 5, 2024

SARS-CoV-2 is an enveloped, positive-sense, single-stranded RNA virus belonging to the genus *Betacoronavirus*. The virus genome consists of approximately 29.9 kilobases, with two untranslated sequences of 254 and 229 bases at the 5'- and 3'-ends, respectively. (3) The viral particle contains at least four structural proteins, including the spike (S) protein, envelope (E) protein, membrane (M) protein, and nucleocapsid (N). (4) To enter human cells, the spike protein mediates the attachment to the host cells by binding to the human angiotensin-converting enzyme 2 (ACE2) receptor and facilitating virus-cell membrane fusion during infection. (5 - 7)

Thus, the spike is considered a key protein for virus invasion and virulence. For disease treatment, an effective approach is blocking the virus from entering the host cells by targeting the spike protein or specific receptors on the host surface. (8)

The B-cell epitope is one of the main targets in the development of vaccines and drug designs because the neutralizing antibodies produced by B cells are an essential part of adaptive immunity by critically participating in neutralizing viruses by blocking virus attachment and entry into cells, thereby preventing infection of host cells. [9]

To identify potential epitopes that can be used as targets for vaccine and drug development, linear B-cell epitopes of SARS-CoV-2 spike protein were predicted and identified by Polyiam K, *et al.* using immunoinformatics approach and validated with COVID-19 convalescent sera. [10] The majority of the B-cell epitopes found in the study were exposed on the surface, and four epitopes (CoV2_S-10, CoV2_S-11, CoV2_S-11.2, and CoV2_S-13) were determined as the most immunodominant epitopes in the receptor binding domain (RBD) subunit.

Although vaccination campaigns have been implemented globally, which decrease the number of confirmed cases, they do not guarantee immunity against the infection, particularly given the rapid emergence of new variants.[11] Thus, finding the potential treatments for patients with COVID-19 is still urgent. Currently, a total of four drugs have been approved by the U.S. Food and Drug Administration (FDA) for the treatment of COVID-19, which included two antiviral drugs, namely, Veklury (remdesivir) and Paxlovid (nirmatrelvir and ritonavir), and two immune modulators, namely, Olumiant (baricitinib) and Actemra (tocilizumab).[12] The use of remdesivir is limited for the treatment of children aged > 28 days and weight > 3 kg and adult patients with mild-to-moderate symptoms who are more likely to become severely ill. [13] Meanwhile, the combination of nirmatrelvir and ritonavir is limited in only adults with mild-to-moderate symptoms. [14] The use of baricitinib and tocilizumab is limited to hospitalized adults that require supplemental oxygen, which means that the patients are already in severe condition.[15, 16] Other drugs, such as molnupiravir, anakinra, and vilobelimab, are given an emergency use authorization, which means that the known and potential benefits of these drugs outweigh their known and potential risks, and there are no suitable alternatives; however, they need to be evaluated further for permanent FDA approval.[12] Because the current medications have some limitations and adverse effects to some patients, specifically senior citizens and those with underlying diseases, the search for potential treatment with the mildest adverse effects remains necessary and worthy of the focus.

The drug discovery process is generally long and complex. It requires extensive screening of large compound libraries, followed by lead optimization and preclinical testing before advancing to clinical trials. [17] In contrast, drug repositioning or drug repurposing uses existing drugs that are already approved or in clinical development for other treatments; thus, making it requires less time and resources than the conventional method. [17] This approach has also been proven to be very efficient and beneficial to COVID-19 treatment, as three-quarters of the current FDA-approved drugs were discovered, including broad-spectrum antiviral drug remdesivir [18, 19], anti-HIV drug booster ritonavir [20], and rheumatoid arthritis drugs baricitinib and tocilizumab.[21, 22] Moreover, some other drugs showed promising results in clinical trials, such as the anticancer drug, sabizabulin [23] and the anti-inflammatory and immunosuppressant agent dexamethasone. [24]

Among the repurposed drugs proposed by researchers, antimalarial drugs, such as chloroquine and hydroxychloroquine were found to exhibit antiviral activities against SARS-CoV-2 *in vitro* and were put forward as one of the promising candidates for COVID-19 treatment in the early pandemic.[25] However, during clinical trials with patients having severe COVID-19 and some of them having underlying diseases, both drugs were not efficacious. [26] In this study, we aimed to identify malaria box compounds capable of binding to and inhibiting the activity of the SARS-CoV-2 spike protein.

Materials and methods

Epitope selection and 3D structure prediction

The SARS-CoV-2 spike protein (accession number 6VSB_A) was retrieved from the National Center for Biotechnology Information database (https://www.ncbi.nlm.nih.gov/protein/). Linear B-cell epitopes were predicted using immunoinformatics programs as described by Polyiam K, *et al*. [10], with 38 predicted linear B-cell epitopes within the spike protein. In that study, eight epitopes located in the receptor-binding domain (RBD) from residues 330 - 535 together with four epitopes in the non-RBD domains were selected and used in further analysis. The non-RBD epitopes were selected based on their location in the N-terminal domain (NTD) and cytoplasmic tail located in S1 and S2 subunits, respectively. The NTDs are exposed on the viral surface and responsible for the initial attachment of

the virus to the host cell surface, facilitating viral entry, whereas the cytoplasmic tail is responsible for membrane fusion and signal transduction, highlighting their importance in viral entry and making them potential targets for therapeutic interventions and drug design.

The three-dimensional structures of the selected epitopes were predicted using the PEP–FOLD3 web-based tool, based on a new hidden Markov model suboptimal conformation sampling approach.[27-29] The output was the representative of the five best clusters ranking from models 1 to 5. The predicted structures were obtained in the PDB format.

In silico molecular docking studies and receptor-ligand interaction analysis

Four hundred malaria box compounds were virtually screened against the 12 epitopes of SARS-CoV-2, including eight epitopes in the RBD and four in the non-RBD regions. Molecular docking was performed using iGEMDOCK v 2.1. [30] The hydrophobic and electrostatic preferences were set at 1.0, and docking was performed using standard settings at 70 generations per compound with a population size of 200 random individuals. The fitness (total free energy) obtained from iGEMDOCK scoring is the summation of van der Waal energy, hydrogen bonding energy, and electrostatic energy. The three top-scoring compounds with the lowest total free energy for each epitope were selected. The best binding pose of each compound was then analyzed and visualized using BIOVIA Discovery Studio 2020 (Dassault Systèmes).

Peptide and protein preparation

For the SPR assay, the peptides of the predicted epitopes were chemically synthesized (Biomatik, USA). The synthetic peptides were dissolved in sterile distilled water containing 0.1% acetic acid to a concentration of 1.5 mg/mL and stored at –20°C until use. The RBD-V5 subunit used in the ELISA assay was produced in the mammalian HEK 293 cell line using the plasmid pVAX1 harboring a gene encoding the SARS-CoV-2 RBD subunit. [10] The RBD-V5 protein was collected from the medium of the transfected HEK 293 culture.

Competitive ELISA

A 96-well microplate (Thermo Fisher Scientific, MA, USA) was coated with 3 µg/mL (50 µl/well) of recombinant human ACE2 (Fc Chimera; ab273687; Abcam) and incubated overnight at 4°C. After three washes with 100 µl/well of phosphate-buffered saline (PBS) containing 0.05% Tween 20 (PBST), the microplate was blocked with 5.0% bovine serum albumin in PBST (BSA/PBST; 100 µl/well) for 1 h at room temperature. After three washes with PBST, 100 µlof 20 µg/mL RBD-V5 pre-incubated with 0.1 mM malaria box compounds for 45 min was added to the plate. In parallel, RBD-V5 (100µl of 20 µg/mL) was added as a control. After 1 h of incubation at room temperature, the plate was washed three times with PBST. Mouse anti-V5 antibody (Invitrogen, CA, USA) diluted 1 : 2,000 was added to the plate (100 µl/well), followed by incubation at room temperature for 1 h. After three washes with PBST, goat-anti-mouse IgG-HRP (Abcam) diluted 1 : 100,000 was added (100 µl /well), and the plate was incubated for 1 h. The plate was washed three times with PBST, and TMB substrate (70 µl/well, Bio-Rad) was then added, with incubation for 30 min at room temperature. In the final step, 2N H_2SO_4 was added (35 µl/well) to stop the reaction of the TMB substrate. Optical density at a wavelength of 450 nm was measured using the Infinite F50 microplate reader (Tecan). The schematic representation of the competitive inhibition of RBD-ACE2 interaction is shown in **Figure 1**. The experiments were conducted in triplicate. The percentage of inhibition was calculated based on the following formula:

Percent inhibition = 100 - [100 × (OD_{450} of RBD with malaria box compounds - OD_{450} of no-RBD)/(OD_{450} of RBD - OD_{450} of no-RBD)]

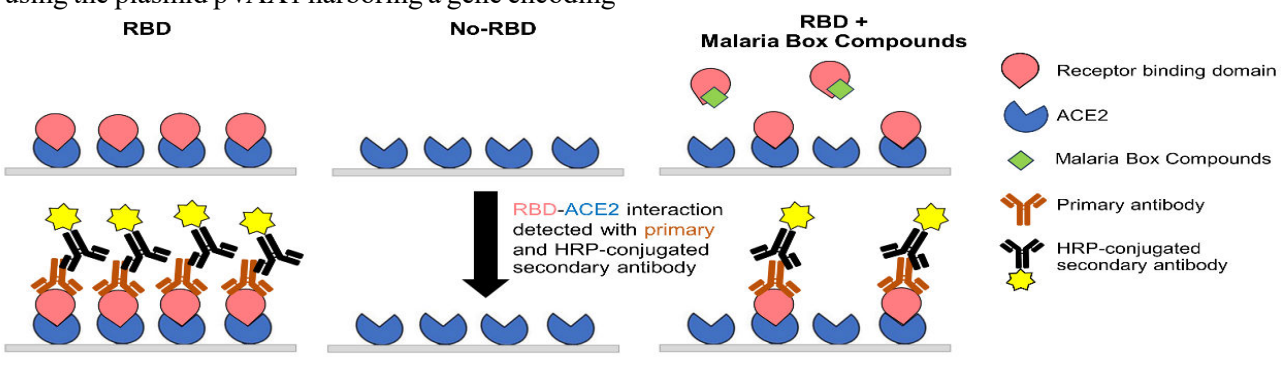

Figure 1. The schematic representation of the competitive inhibition of RBD-ACE2 interaction.

Binding affinity of malaria box compounds to non-RBD epitopes (SPR assay)

The binding affinities of the non-RBD epitope peptides, including CoV2_S-1.2, CoV2_S-2, CoV2_S-3, and CoV2_S-21.2, to the malaria box compounds MMV007384, MMV019881, MMV667488, MMV007092, MMV011895, MMV085583, MMV000753, and MMV020912 were examined using Nicoya Amine Sensor Chips (NH_2-Au-100) and Amine Coupling kits with the one-channel OpenSPR starter kit (Nicoya Lifesciences). The malaria box compounds were obtained from Nguitragool W. (Department of Molecular Tropical Medicine and Genetics, Faculty of Tropical Medicine, Mahidol University, Thailand). Filtered-sterile and degassed PBS containing 1.0% DMSO was used as the diluting and running buffer for MMV007092 and MMV011895, whereas PBS containing 0.5% DMSO was used as the running buffer for other analytes. To generate covalent coupling with the Amine Sensor Chip, the SARS-CoV-2 epitope peptides synthesized by Biomatik (USA) were first activated by adding COOH and Nicoya activation buffer and then incubated in a 1:1 carbodiimide and succinimide (ECD/NHS) mixture for 1 h following the manufacturer's instructions. Peptides at a concentration of 50 µg/ml were then injected at a flow rate of 20 µl/min for 5 min, followed by blocking with the blocking solution from the Nicoya Amine Coupling kits to complete the ligand immobilization step. The immobilization levels were approximately 600-700 RU. To determine the binding kinetics, the analytes and malaria box compounds were prepared in a twofold serial dilution from 0.039 to 10 µM. All experiments were performed at 20°C, and each dilution was injected at a flow rate of 30 µl/min for 3 min of association, followed by 5 min of dissociation. After the dissociation, the analytes were removed from the immobilized surface by injecting regeneration buffer (2 M $MgCl_2$) for 1 min, followed by PBS in every injection. The SPR responses were fitted to a 1:1 Langmuir interaction model. The kinetics of the interaction between the malaria box compounds and peptide-bound sensor chip were evaluated using Tracedrawer 1.9.2 (Ridgeview Instruments), and the binding kinetics and equilibrium dissociation constant ($K_D = k_d/k_a$) were calculated based on the association rate constant (k_a) and dissociation rate constant (k_d) of the ligand compound.

Statistical analysis

Statistical analysis was performed using the one-way analysis of variance, followed by the pairwise post-hoc Tukey HSD test using Microsoft Excel's Data Analysis ToolPak and online web statistical calculators (https://astatsa.com/). $P < 0.05$ was considered statistically significant, and $P < 0.01$ was considered highly significant.

Results

Epitope selection and 3D structure prediction

From a previous study by Polyiam K, *et al*. [10], linear B-cell epitopes were identified in 21 regions of the SARS-CoV-2 spike protein using an immunoinformatics approach. The predicted epitopes from that study were then selected and used in the present study, which included eight and four epitopes in the RBD and non-RBD regions, respectively. The eight epitopes in the RBD included CoV2_S-8, 9, 10, 11.1, 11.2, 12.1, 12.2, and 13, of which CoV2_S-11.2, 12.1, and 12.2 are located in the region involved in ACE2 receptor binding. [10] Of the other four epitopes, CoV2_S-1.2, 2, and 3 are located in the S1 N-terminal domain (NTD), whereas CoV2_S-21.2 is located in the cytoplasmic tail, which is part of the S2 subunit of the spike protein. The amino acid sequences and location of the selected epitopes on the spike protein are shown in **Table 1** and **Figure 2A**. The predicted 3D models of all 12 epitopes are illustrated in **Figure 2B-2D**.

In silico molecular docking studies and receptor-ligand interaction analysis

In silico molecular docking was performed to analyze the interaction between the epitope peptides and malaria box compounds. The compounds interacting with each epitope were ranked based on total free energy. The top three compounds against each epitope are shown in **Table 2**. Of these compounds, MMV019881 showed the lowest free energy when interacting with epitope CoV2_S-3 (- 106.44 kcal/mol) and CoV2_S-2 (- 105.321 kcal/mol). On the contrary, MMV000563 showed the lowest total free energy (- 100.708 kcal/mol) when interacting with CoV2_S-8, whereas MMV665943 showed the highest total free energy (- 64.901 kcal/mol) with CoV2_S-9. The binding interactions between the epitopes and compounds obtained from *in silico* molecular docking are illustrated in **Figure 3A - 3D**.

Table 1. Predicted epitopes from the SARS-CoV-2 spike protein chosen for this study.

Epitope name	Sequence	Length	Residues
CoV2_S - 1.2	VYYPDKVFR	9	36 - 44
CoV2_S - 2	FSNVTWFHAIHVSGTNGTKRFDN	23	59 - 81
CoV2_S - 3	LGVYYHKNNKSWMESEFRVYSSA	23	141 - 163
CoV2_S - 8	NITNLCPFGEVFNATRFASVYAWNRKRI	28	331 - 358
CoV2_S - 9	GVSPTKLNDL	10	380 - 389
CoV2_S - 10	GDEVRQIAPGQTGKIADYNYK	21	404 - 424
CoV2_S - 11.1	NNLDSKVGGNYNYLYR	16	439 - 454
CoV2_S - 11.2	LFRKSNLKPFERDISTEIYQAGST	24	455 - 478
CoV2_S - 12.1	VEGFNCYFPLQ	11	483 - 493
CoV2_S - 12.2	GFQPTNGVGYQP	12	496 - 507
CoV2_S - 13	ELLHAPATVCGPKKSTNLVK	20	516 - 535
CoV2_S - 21.2	SCCKFDEDDSEPVLKGVKL	19	1252 - 1270

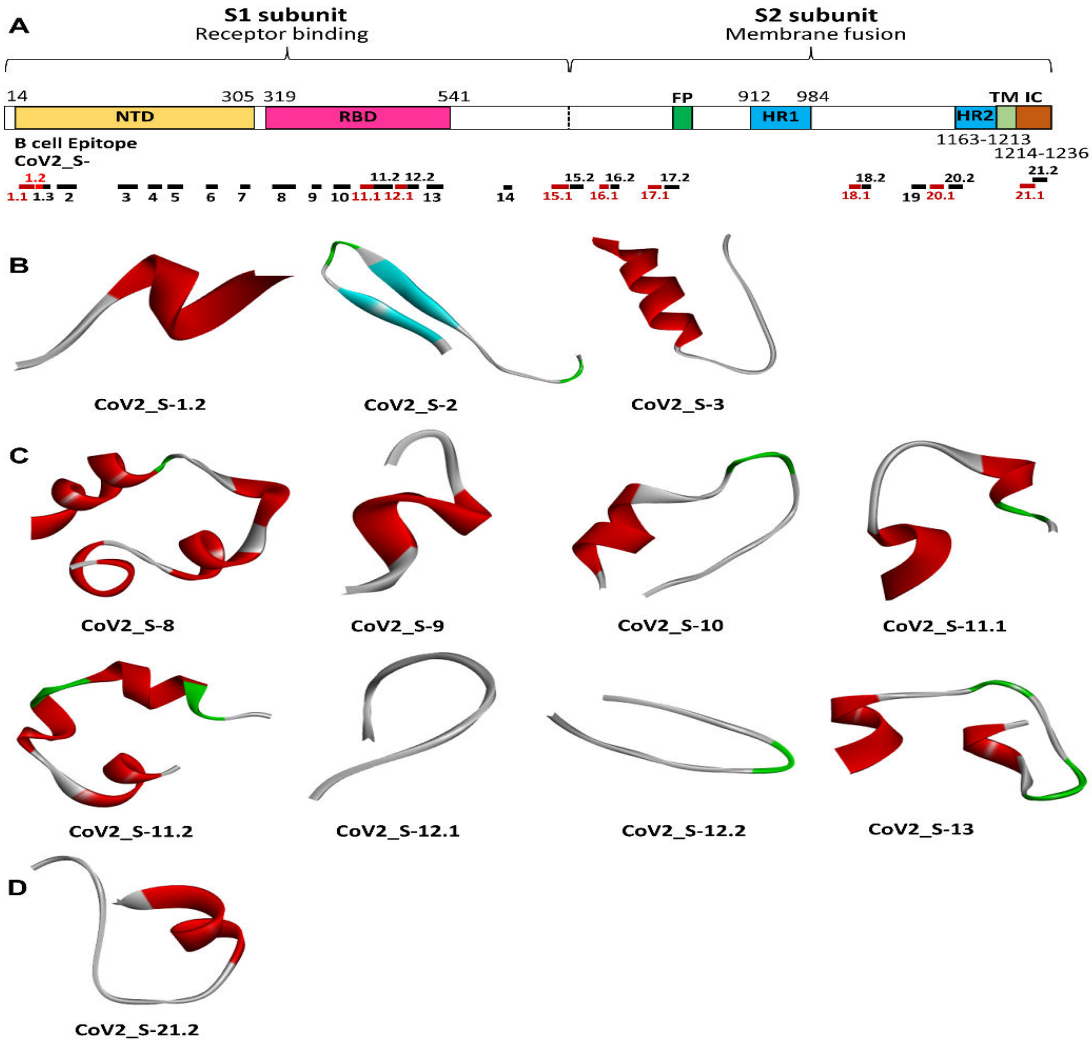

Figure 2. Location of predicted linear B-cell epitopes on the SARS-CoV-2 Spike protein and predicted 3-D structure of each epitope. **(A)** Composition of the spike protein and locations of the predicted linear B-cell epitope; **(B - D)** Predicted protein structure of predicted linear B-cell epitopes. The 3D structure of the epitopes located in the N-terminal domain (NTD) **(B)**; receptor- binding domain (RBD) **(C)**; and Intracellular tail (IC) **(D)** are shown. Different secondary structures are labeled in different colors; red represented helix, white represented coil, green represented turn, and blue represented sheet.

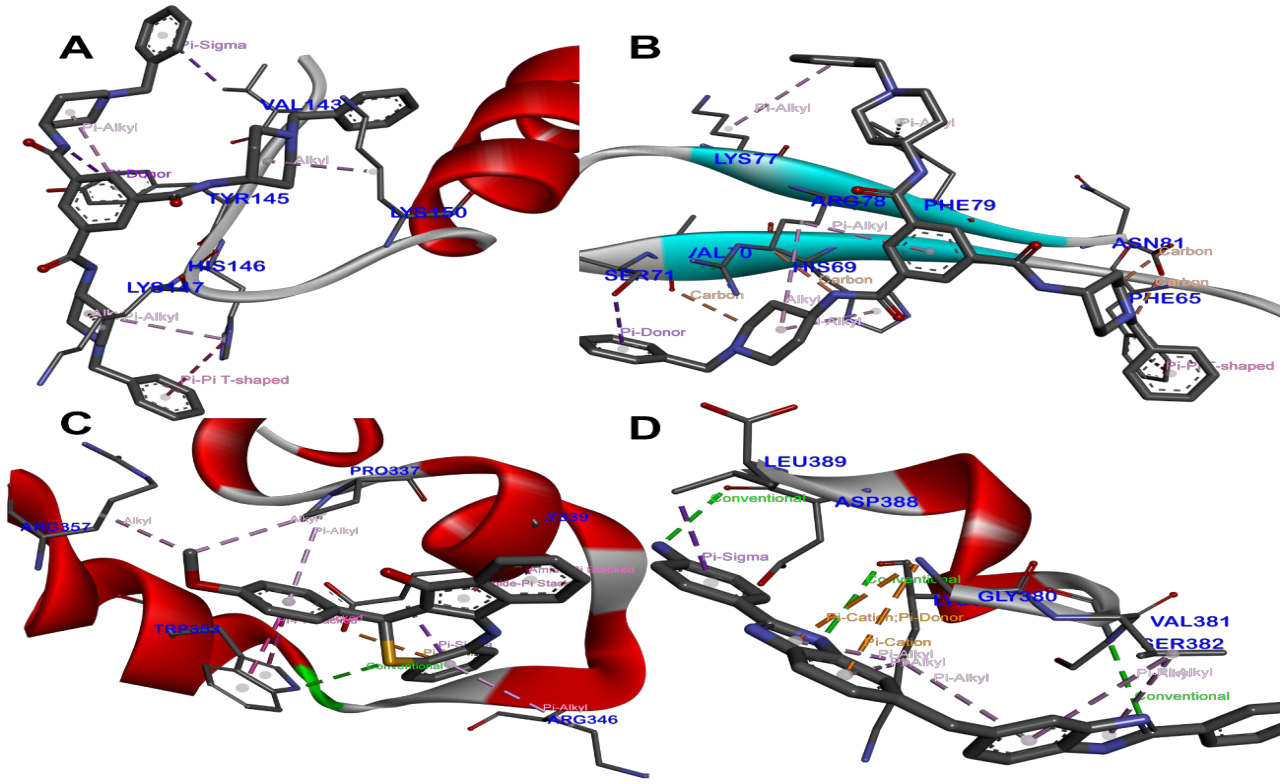

Figure 3. Three-dimensional model of the interaction between the compounds and predicted B-cell epitopes in the RBD. Interactions between a compound and its target epitope are shown as follows: (**A**) MMV019881 and CoV2_S-3; (**B**) MMV019881 and CoV2_S-2; (**C**) MMV000563 and CoV2_S-8; and (**D**) MMV665943 and CoV2_S-9.

Table 2. Summary of the top 3 malaria box compounds that exhibit the lowest total energy (kcal/mol) when analyzed by *in silico* molecular docking and their amino acid residues of interactions.

	Total free energy (kcal/mol)	Interacting amino acid residues			
		H-bond	Halogen (Fluorine)	Electrostatic bonds	Others
CoV2_S - 1.2					
MMV007384	-85.3045	-	-	-	Pro39, Val42, Phe43
MMV665943	-84.9518	-	-	-	Pro39, Val42
MMV011895	-84.7239	Asp40	-	Asp40	Pro39, Lys41, Val42, Phe43, Arg44
CoV2_S - 2					
MMV019881	-105.321	Val70, Ser71, Arg78, Asn81	-	-	Phe65, His69, Lys77, Phe79
MMV011895	-88.0976	Asn81	-	-	Ile68, His69, Arg78, Phe79
MMV667488	-83.3115	His66, Ile68, His69, Val70	-	-	Ala67
CoV2_S - 3					
MMV019881	-106.44	Tyr145	-	-	Val143, His146, Lys147, Lys150
MMV000753	-97.4296	Lys147	-	-	Leu141, Val143, Tyr144, Tyr145, Lys150
MMV085583	-96.1185	Val143	-	-	Tyr144, Tyr145, Lys150, Met153, †Glu156, Phe157, Tyr160

Table 2. (Cont.) Summary of the top 3 malaria box compounds that exhibit the lowest total energy (kcal/mol) when analyzed by *in silico* molecular docking and their amino acid residues of interactions.

	Total free energy (kcal/mol)	Interacting amino acid residues			
		H-bond	Halogen (Fluorine)	Electrostatic bonds	Others
CoV2_S - 8					
MMV000563	- 100.708	Trp353	-	Glu340	Pro337, Gly339, Arg346, Arg357
MMV019690	- 100.001	Glu340, Trp353	Lys356	-	Arg346, Arg357
MMV665814	- 98.755	-	-	Glu340	Pro337, Arg346, Trp353
CoV2_S - 9					
MMV011895	- 66.5846	-	-	Asp388	Thr384, Lys385, Leu389
MMV019738	- 65.3073	Gly380	-	Gly380	Val381, Lys385, Asp388, Leu389
MMV665943	- 64.9011	Gly380, Ser382, Lys385, Asp388	-	Gly380	Val381, Leu389
CoV2_S - 10					
MMV665881	- 79.6419	Arg408, Gln414, Lys417, Asp420	-	Arg408, Asp420	Pro412
MMV085471	- 79.5174	Gly416	-	-	Pro412, Lys417, Ile418
MMV007384	- 79.2539	-	-	-	Ala411, Tyr423
CoV2_S - 11.1					
MMV007591	- 82.9289	-	-	-	Leu441, Val445, Asn448, Tyr451, Leu452
MMV665814	- 82.7192	Tyr449	-	Asp442	Leu441, Val445, Gly447, Leu452
MMV007160	- 81.8378	Asp442, Gly447, Asn448	-	-	Leu441, Tyr449, Leu452
CoV2_S - 11.2					
MMV019881	- 91.7719	Ser459	-	Glu465, Arg466	Leu455, Lys458, Lys462, Tyr473
MMV085471	- 88.223	-	-	-	Lys462, Glu465, Arg466, Tyr473
MMV665881	- 87.7063	Lys458, Glu465	-	-	Lys462, Arg466, Tyr473
CoV2_S - 12.1					
MMV011895	- 89.9836	Val483, Asn487	-	Glu484	Cys488, Pro491
MMV666023	- 83.0161	Tyr489	-	-	Val483, Pro491
MMV007384	- 82.8648	Leu492, Gln493	-	-	Val483, Pro491
CoV2_S - 12.2					
MMV011895	- 79.372	Gln498, Tyr505	-	-	Pro499, Val503
MMV019881	- 72.6968	Thr500, Pro507	-	-	Pro499, Val503, Tyr505
MMV000720	- 72.4871	Gly504, Tyr505, Gln506	-	-	Pro499, Val503

Table 2. (Cont.) Summary of the top 3 malaria box compounds that exhibit the lowest total energy (kcal/mol) when analyzed by *in silico* molecular docking and their amino acid residues of interactions.

	Total free energy (kcal/mol)	Interacting amino acid residues			
		H-bond	Halogen (Fluorine)	Electrostatic bonds	Others
CoV2_S - 13					
MMV000662	-88.6775	Lys529, Leu533	-	Lys529	Leu517, His519, Ala522, Val534
MMV666023	-86.2064	-	-	-	Leu517, Leu518, Pro521, Ala522, Cys525, Lys529, Leu533
MMV011895	-84.3351	-	-	-	Ala520, Pro521, Ala522, Val524
CoV2_S - 21.2					
MMV665977	-95.7304	-	Phe1256	Asp1257, Glu1262	Lys1255, Leu1265
MMV020912	-93.7202	Lys1255	-	Glu1262	Phe1256, Asp1257, Leu1265
MMV007384	-90.0206	Ser1261	-	Asp1257, Glu1262	Lys1255, Leu1265

† represents unfavorable bump.

Interestingly, MMV011895 could bind to six predicted epitopes (CoV2_S-1.2, 2, 9, 12.1, 12.2, and 13) with low total free energy, whereas MMV019881 could bind to four epitopes (CoV2_S-2, 3, 11.2, and 12.2) and MMV007384 could bind to four epitopes (CoV2_S-1.2, 10, 12.1, and 21.2). Furthermore, four compounds could bind to two epitopes, including MMV085471, MMV665881 (CoV2_S-10 and 11.2), MMV665814 (CoV2_S-8 and 11.1), and MMV665943 (CoV2_S-1.2 and 9), MMV666023 (CoV2_S-12.1 and 13). These results suggest the potential of malaria box compounds for binding to and inhibiting the activity of the SARS-CoV-2 spike protein, particularly MMV011895, MMV019881, and MMV007384 because they can interact with multiple epitopes of the spike protein, thus potentially increasing their inhibition efficiency compared with other compounds that interact with only one epitope. Importantly, because the predicted epitopes CoV2_S-12.1 and CoV2_S-12.2 possess the residues required for receptor recognition, the compound interacting with these regions may inhibit viral entry with great efficiency.

Competitive ELISA

Based on the *in silico* molecular docking results, seven malaria box compounds were tested for their inhibitory effect on the spike RBD using competitive ELISA. This included two compounds (MMV000563 and MMV019690) exhibiting the lowest free energy against spike RBD, four compounds (MMV007384, MMV085471, MMV665881, and MMV011895) that showed the potential to interact with multiple RBD epitopes, and one compound (MMV665943) that exhibited the highest free energy against RBD. The results showed that the interaction between the RBD and ACE2 decreased in the presence of malaria box compounds (**Figure 4A**), suggesting their capacity for inhibiting the interaction between the spike RBD and its receptor ACE2. The percent inhibition of the RBD-ACE2 interaction by malaria box compounds is shown in **Table 3** and **Figure 4B**. Of the seven compounds, MMV665881 exhibited the highest percent inhibition of 55.4%. According to *in silico* molecular docking, MMV665881 potentially interacts with CoV2_S-10 and CoV2_S-11.2 **(Table 2)** by forming hydrogen bonds with Arg408, Gln414, Lys417, and Asp 420 residues and Pi-Akyl interaction with Pro412 in CoV2_S-10 and forming hydrogen bonds with Lys458 and Glu465 and Pi-Akyl interactions with Lys462, Arg466, and Tyr473 in CoV2_S-11.2. The 3D model of MMV665881 interacting with residues in CoV2_S-10 and CoV2_S-11.2 is presented in **Figure 5**. Although MMV011895 was predicted by molecular docking to interact with four epitopes within the RBD (CoV2_S-9, 12.1, 12.2, and 13), its percent

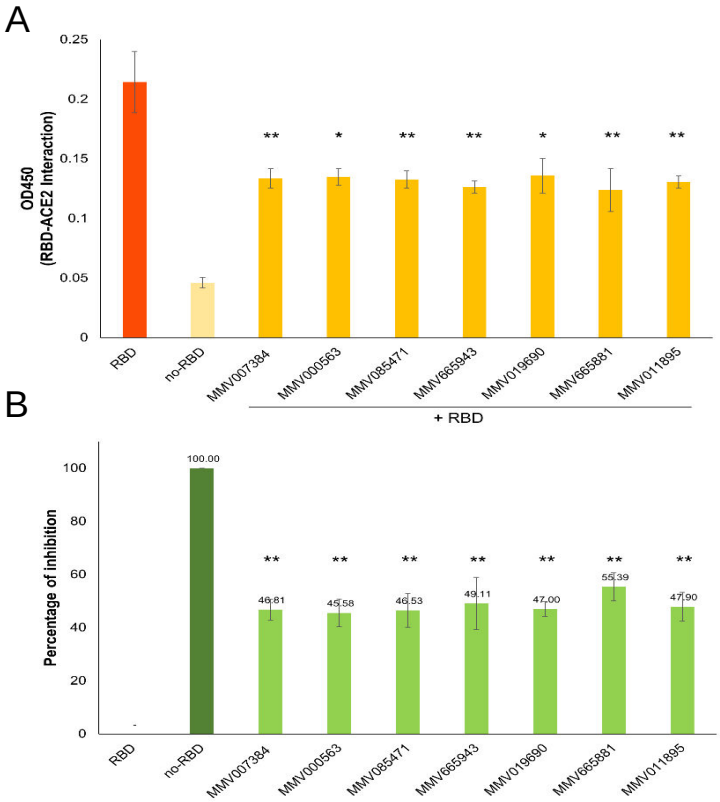

Figure 4. RBD inhibition by 7 malaria box compounds measured by competitive ELISA. Interaction between the RBD and ACE2 was measured using ELISA. Seven malaria box compounds showing high binding affinity by *in silico* molecular docking were added into the reaction to compete with ACE2 in binding to RBD. **(A)** Effects of malaria box compounds in inhibiting RBD-ACE2 interaction; **(B)** Ability of the compounds to inhibit the RBD-ACE2 interaction was then analyzed and shown as % inhibition. Data presented by mean ± SEM (error bar). One-way ANOVA with post-hoc Tukey HSD test was used in statistical analysis. "*" and "**" indicates a significant difference between the conditions with and without malaria box compounds with $P < 0.05$ and $P < 0.01$, respectively. The experiment was carried out in triplicate.

Table 3. The inhibitory effect of the malaria box compounds on the RBD-ACE2 interaction, and the predicted epitopes involved in the interaction.

Malaria box compounds	% Inhibition activity	RBD epitopes of interaction CoV2_
MMV007384	46.8 ± 4.0	S - 10, S - 12.1
MMV000563	45.6 ± 5.2	S - 8
MMV085471	46.5 ± 6.3	S - 10, S - 11.2
MMV665943	49.1 ± 9.8	S - 9
MMV019690	47.0 ± 2.8	S - 8
MMV665881	55.4 ± 5.3	S - 10, S - 11.2
MMV011895	47.9 ± 5.4	S - 9, S - 12.1, S - 12.2, S - 13

Competitive ELISA was performed with 7 malaria box compounds targeting RBD chosen based on molecular docking results. Data presented by mean ± standard error of mean (SEM). The experiment was repeated 3 times and performed in 3 replicates.

inhibition was only 47.9%. The 3D model of MMV011895 interacting with residues in CoV2_S-9, CoV2_S-12.1, CoV2_S-12.2, and CoV2_S-13 is presented in **Figure 6**. In the presence of MMV665881 ($P = 0.004$), MMV665943 ($P = 0.005$), MMV011895 ($P = 0.007$), MMV085471 ($P = 0.009$), and MMV007384 ($P = 0.0099$), the decrease in RBD-ACE2 interaction was highly significant when compared with the control group. Meanwhile, the addition of MMV000563 and MMV019690 decreased the RBD-ACE2 interaction significantly ($P = 0.011$ and $P = 0.012$, respectively). Altogether, the ability of the studied compounds to inhibit the RBD–ACE2 interaction is ranked as follows: MMV665881 > MMV665943 > MMV011895 > MMV019690 > MMV007384 > MMV085471 > MMV000563. However, even though seven malaria box compounds showed a significant difference relative to the control, no significant difference was found relative to each other.

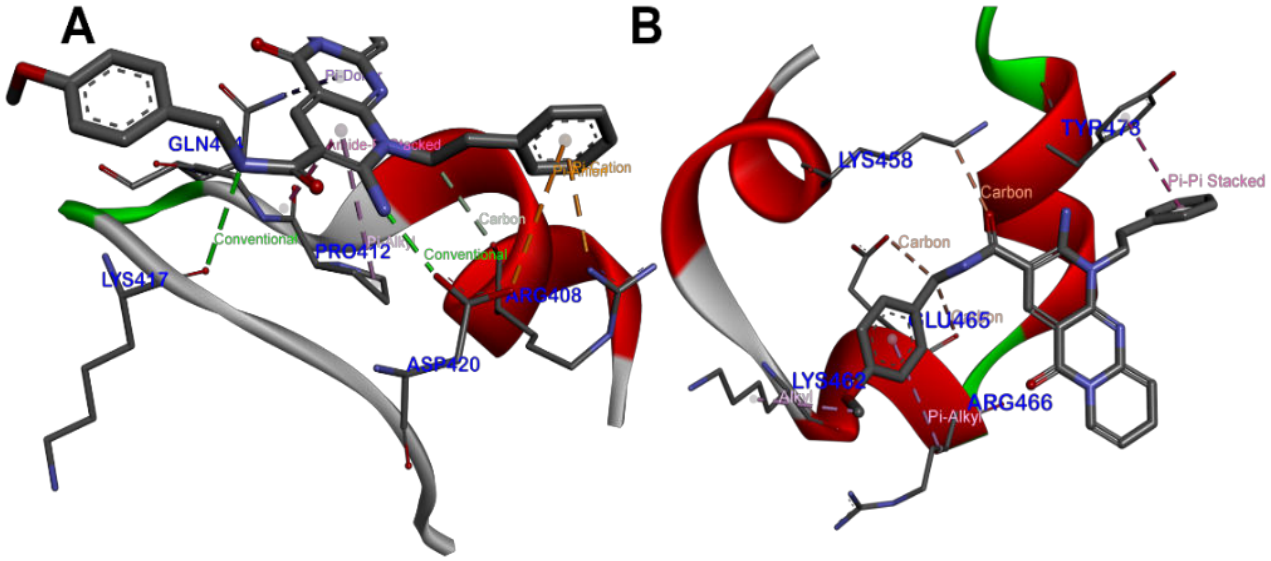

Figure 5. Three-dimensional model representing the interaction between the compound MMV665881 and its target RBD epitopes. The MMV665881 compound, which exhibited the highest RBD inhibition, was analyzed for its interaction with 2 epitopes in the RBD: **(A)** CoV2_S-10 and **(B)** CoV2_S-11.2.

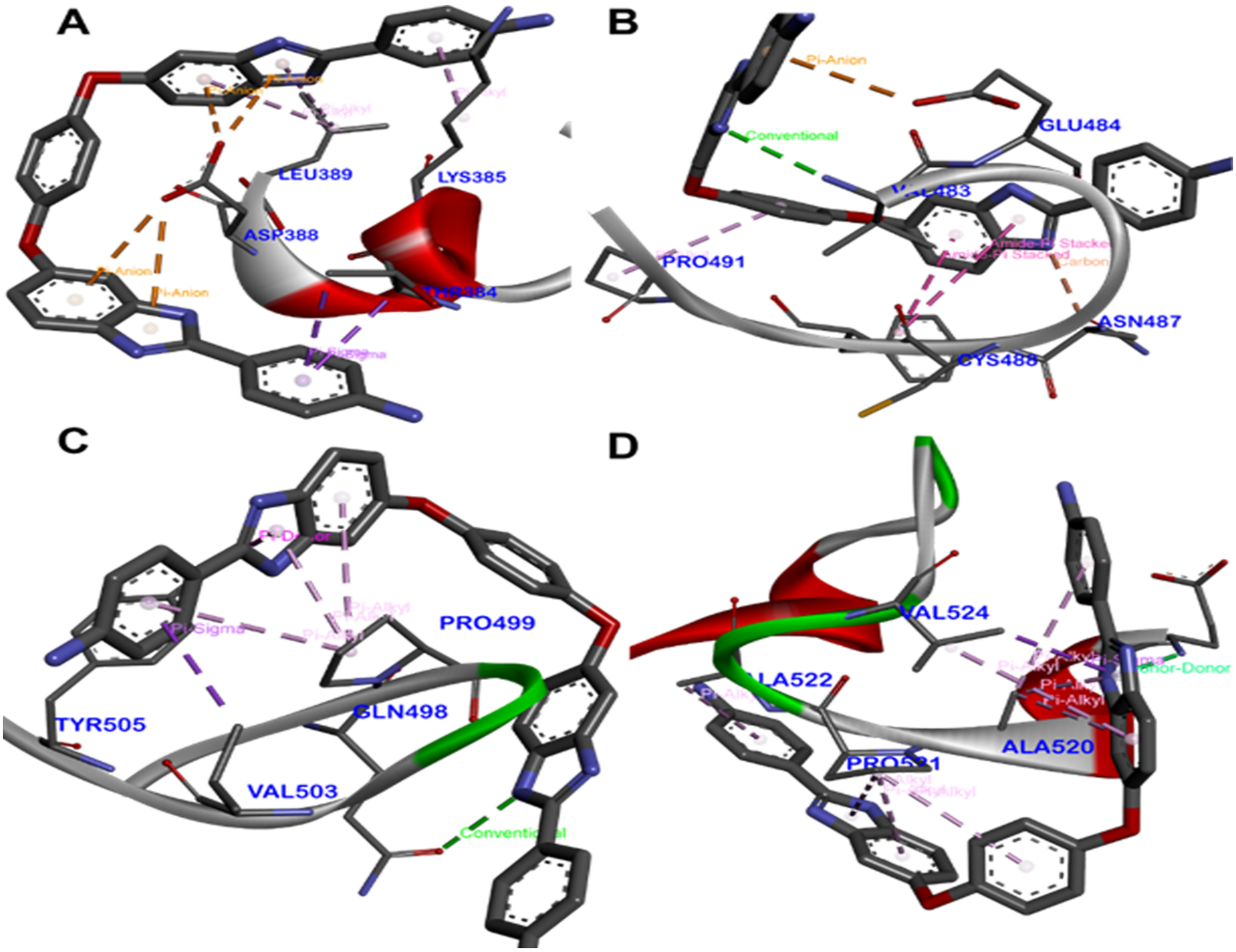

Figure 6. Three-dimensional model representing the interaction between the MMV011895 compound and its RBD epitopes. The MMV011895 compound, the second-ranked compound capable of inhibiting the RBD-ACE2 interaction, was analyzed for its interaction with its 4 RBD epitopes: **(A)** CoV2_S-9; **(B)** CoV2_S-12.1; **(C)** CoV2_S-12.2; and **(D)** CoV2_S-13.

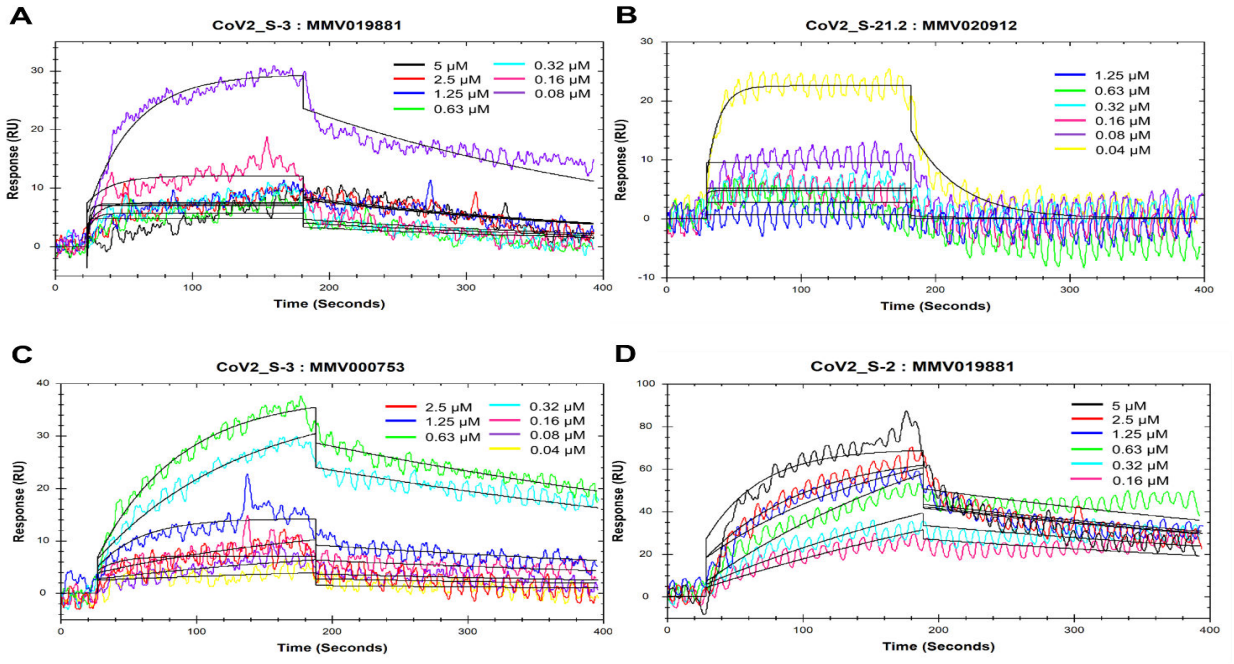

Figure 7. The sensorgrams of surface plasmon resonance (SPR) generated with Trace Drawer 1.9.2 software (ridgeview instruments). The SPR assay was performed with epitope peptides and chosen compounds. Four synthetic peptides corresponding to the epitopes located in the non-RBD region were captured on Amine sensor chip at immobilization level of 600-700 RU. Various concentration (as indicated) of 8 malaria box compounds were injected at flow rate of 30 µl/min in running buffer. Colors of injection curves are matched with corresponding concentrations. Fitted curves (black lines) are superimposed over all experimental curves using 1 : 1 Langmuir interaction model. The binding between the compounds and their target epitopes are shown as follows: **(A)** CoV2_S-3 and MMV019881; **(B)** CoV2_S-21.2 and MMV020912; **(C)** CoV2_S-3 and MMV000753; **(D)** CoV2_S-2 and MMV019881.

Binding affinity of malaria box compounds to non-RBD epitopes

In addition to the RBD-binding compounds, malaria box compounds capable of binding to epitopes located in non-RBD regions were also examined using the SPR assay. The eight malaria box compounds (MMV020912, MMV07384, MMV019881, MMV011895, MMV667488, MMV007092, MMV000753, and MMV085583) selected for the SPR assay were selected in accordance with their binding stability with the epitopes (**Table 2**). The binding affinities of the compounds to their target epitopes were determined by the equilibrium dissociation rate constants (K_D) (**Table 4**). The examples of SPR sensorgram patterns of three compounds (MMV019881, MMV020912, and MMV000753) and their target epitopes are demonstrated in **Figure 7**. MMV020912 showed high affinity for CoV2_S-21.2, with a K_D value of $1.4 \pm 0.0 \times 10^{-8}$. Meanwhile, MMV019881, MMV667488, MMV007092, and MMV011895 showed moderate interactions with CoV2_S-2. MMV019881, MMV085583, and MMV000753 showed interaction with CoV2_S-3. These results suggest the possibility of malaria box compounds acting as inhibitors of SARS-CoV-2 spike protein. The 3D models of interaction between the three top compounds (MMV019881, MMV020912, and MMV000753) and their target epitopes are presented in **Figure 3A - 3B** and **Figure 8**. MMV019881 interacts with CoV2_S-3 by forming a hydrogen bond and a non-covalent bond, Pi-alkyl interaction with Tyr145, Pi-Sigma with Val143, Pi-Pi T-shaped and Pi-alkyl interactions with His146, and alkyl interaction with Lys147 and Lys150 (**Figure 3A**). It also forms hydrogen bonds with Val70, Ser71, Arg78, and Asn81, Pi-Pi T-shaped with Phe65, alkyl interaction with Arg78, and Pi-alkyl interactions with four amino residues, namely, His69, Lys77, Arg78, and Phe79, in CoV2_S-2 (**Figure 3B**). MMV020912 interacts with CoV2_S-21.2 by forming a hydrogen bond and Pi-alkyl interaction with Lys1255, an electrostatic bond with Glu1262, Pi-sigma bond with Asp1257, Pi-Pi stacked with Phe1256, and Pi-alkyl interactions with Leu1265 (**Figure 8A**). MMV000753 interacts with CoV2_S-3 by forming a hydrogen bond with Lys147, Pi-sigma, Pi-lone pair, and Pi-alkyl interactions with Val143, Pi-Pi stacked and Pi-Pi T-shaped with Tyr145, Pi-Pi T-shaped with Tyr144, and Pi-alkyl interactions with Leu141 and Lys150 (**Figure 8B**).

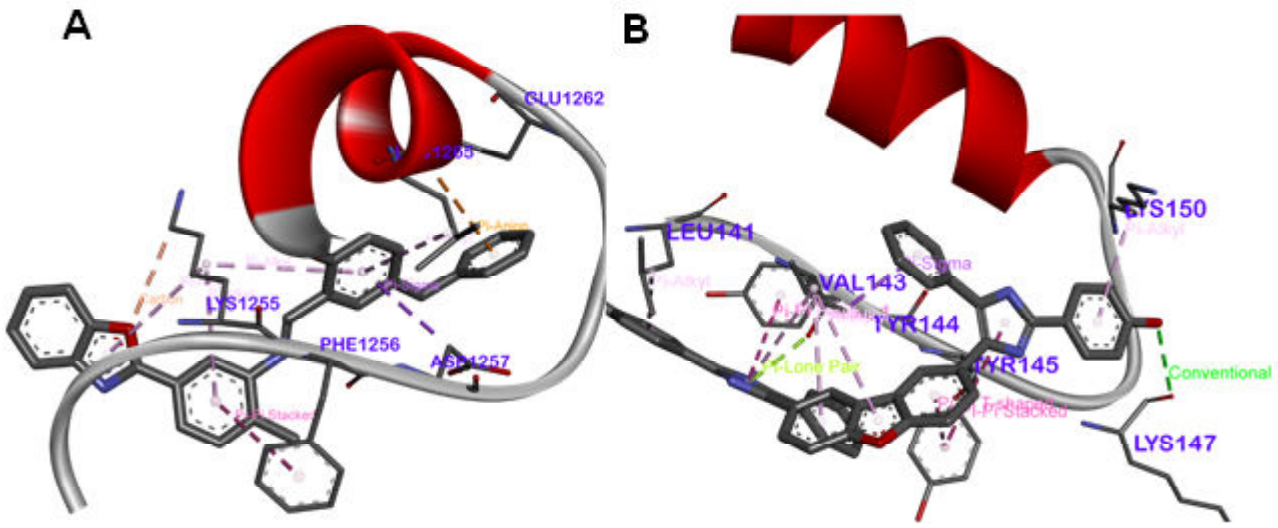

Figure 8. Three-dimensional model representing the interaction between the compounds and their non-RBD target epitopes. The interaction between **(A)** MMV020912 and CoV2_S-21.2; and **(B)** MMV000753 and CoV2_S-3 are shown.

Table 4. Binding parameters of eight selected malaria box compounds obtained from surface plasmon resonance (SPR) and analyzed with TraceDrawer 1.9.2 software (ridgeview instruments)

	k_a (1/(M*s))	est. error	k_d (1/s)	est. error	K_D (M)	est. error
CoV2_S - 1.2						
MMV007384	1.4×10^{3}	$\pm 8.0 \times 10^{2}$	2.6×10^{-3}	$\pm 1.2 \times 10^{-4}$	1.8×10^{-6}	$\pm 1.6 \times 10^{-6}$
CoV2_S - 2						
MMV019881	5.1×10^{3}	$\pm 2.0 \times 10^{2}$	1.7×10^{-3}	$\pm 1.4 \times 10^{-5}$	3.3×10^{-7}	$\pm 1.5 \times 10^{-8}$
MMV667488	5.0×10^{3}	$\pm 1.2 \times 10^{2}$	1.0×10^{-2}	$\pm 1.2 \times 10^{-6}$	2.0×10^{-6}	$\pm 4.8 \times 10^{-8}$
MMV007092	2.0×10^{3}	$\pm 3.3 \times 10^{2}$	4.5×10^{-2}	$\pm 2.8 \times 10^{-6}$	2.3×10^{-5}	$\pm 4.0 \times 10^{-6}$
MMV011895	6.1×10^{3}	$\pm 3.0 \times 10^{2}$	1.0×10^{-1}	$\pm 3.2 \times 10^{-6}$	1.7×10^{-5}	$\pm 8.2 \times 10^{-7}$
CoV2_S - 3						
MMV019881	3.3×10^{5}	$\pm 1.2 \times 10^{3}$	3.5×10^{-3}	$\pm 4.3 \times 10^{-5}$	1.1×10^{-8}	$\pm 1.7 \times 10^{-10}$
MMV085583	7.1×10^{3}	$\pm 3.1 \times 10^{2}$	5.3×10^{-3}	$\pm 5.7 \times 10^{-6}$	7.5×10^{-7}	$\pm 3.3 \times 10^{-8}$
MMV000753	2.3×10^{4}	$\pm 1.8 \times 10^{2}$	1.9×10^{-3}	$\pm 8.4 \times 10^{-6}$	8.0×10^{-8}	$\pm 9.6 \times 10^{-10}$
CoV2_S - 21.2						
MMV020912	2.0×10^{6}	$\pm 9.1 \times 10^{3}$	2.9×10^{-2}	$\pm 2.0 \times 10^{-4}$	1.4×10^{-8}	$\pm 1.7 \times 10^{-10}$

The binding affinity (K_D); association rate (k_a) and dissociation rate (k_d) for the interactions were determined by SPR analysis.

Discussion

The spike protein is the major target for drug and vaccine development against SARS-CoV-2 because of its receptor recognition function for virus entry using the RBD, which binds to the host cell receptor ACE2. To address the possibility of repurposing malaria box compounds for COVID-19 treatment, in this study, we tested 12 predicted epitopes from the SARS-CoV-2 spike protein (eight and four epitopes in the RBD and non-RBD regions, respectively) reported by Polyiam K, *et al*. [10] The *in silico* molecular docking was used to virtually examine the potential binding forces of malaria box compounds to the spike epitopes and then confirming their interactions using competitive ELISA and SPR assays.

MMV665881 caused the highest inhibition of the RBD-ACE2 interaction, with 55.4% inhibition. *In silico* molecular docking demonstrated that MMV665881 ranked first in interacting with CoV2_S-11.2, with the highest binding affinity (-87.7063 kcal/mol) and second in interacting with CoV2_S-10 (-79.6419 kcal/mol). These epitopes are located within the RBD and have been identified as immunodominant epitopes within this domain; CoV2_S-11.2 was demonstrated to be more immunogenic than CoV2_S-10. [10] These findings suggest that the residues in these two epitopes are vital for the RBD-ACE2 interaction; thus, binding of the compounds to these two epitopes may result in the inhibition of RBD activity in binding to ACE2.

MMV011895 also had an inhibitory effect on the RBD-ACE2 interaction, with 47.9% inhibition. Based on *in silico* molecular docking, this compound interacts with four epitopes in the RBD (CoV2_S-9, CoV2_S-12.1, CoV2_S-12.2, and CoV2_S-13) and two other epitopes located in the NTD region (CoV2_S-1.2 and CoV2_S-2). Thus, MMV011895 may be a promising candidate for SARS-CoV-2 inhibition because of its ability to interact with multiple vital sites on the protein, which may mediate the more extensive inhibition of different variants. However, because competitive ELISA was conducted with a recombinant RBD subunit, the actual inhibitory effect of MMV011895 still needs to be investigated using a viral cell entry model.

MMV007384 and MMV085471 exhibited similar inhibitory effects on the RBD-ACE2 interaction, with percent inhibition values of 46.8% and 46.5%, respectively. MMV007384 was predicted by molecular docking to interact with high binding affinity to CoV2_S-10 and CoV2_S-12.1 within the RBD. Similarly, MMV085471 was predicted to interact with two RBD epitopes but in different regions consisting of CoV2_S-10 and CoV2_S-11.2. In addition, MMV007384 can interact with CoV2_S-1.2 and CoV2_S-21.2 located in the S1 NTD and intracellular tail region, respectively, indicating its versatility and potential for SARS-CoV-2 inhibition.

MMV011895 (4,4'-[benzene-1,4-diylbis(oxy-1H-benzimidazole-5,2-diyl)]dianiline) and MMV007384 (2-(4methoxyphenyl)-5-{[2-(4-methoxyphenyl)-1H-benzimidazol-5-yl]methyl}-1H-benzimidazole) are benzimidazole-based compounds that each contain a guanidine moiety, can act as inhibitors of the heme detoxification pathway of β-hematin formation in *Plasmodium falciparum* [31], and have activity against early- and late-stage gametocytes. [32 - 35] Because it displays rapid killing kinetics against *P. falciparum,* MMV011895 is considered a rapidly parasiticidal antimalarial compound. [36] Based on its molecular structure, MMV011895 contains four H-bond donors, six H-bond acceptors, and six rotatable bonds, which may facilitate the molecular interactions between the compound and multiple sites on the SARS-CoV-2 spike protein.

Azonapthyl benzimidazole or MMV666023 (N-{1-[(1-benzyl-1H-benzimidazol-2-yl) diazenyl]-2-naphthyl}-N-phenylamine), another benzimidazole inhibitor, is a highly hydrophobic probe-like compound with naphthalene and benzimidazole moieties. [37] In previous studies, MMV666023 displayed a high inhibition rate against deoxyhypusine hydroxylase in hypusine synthesis [38] and *P. Falciparum* M1 and M17 aminopeptidases [37], indicating its high potential as an antimalarial drug. However, MMV666023 showed no significant inhibitory effects against other organisms, including *Mycobacteria, Schistosoma,* and *Onchocerca.* [38] MMV666023 contains one H-bond donor, four H-bond acceptors, and six rotatable bonds. Despite having fewer H-bond donors and acceptors, MMV666023 may form conventional hydrogen bonds with Tyr489 of CoV2_S-12.1 as well as nine hydrophobic interactions with seven amino acid residues of CoV2_S-13, resulting in low free energy and a high binding affinity of the protein–ligand interaction.

In this study, *in silico* molecular docking showed that MMV011895, MMV007384, and MMV666023 bind to CoV2_S-12.1 by interacting with the residues

Val483 and Pro491. In addition, MMV011895 and MMV666023 interact with CoV2_S-13 via Pro521 and Ala522, which may suggest the sensitivity of CoV2_S-12.1 and CoV2_S-13 to benzimidazole-based compounds. However, MMV007384 was reported to be a bilayer-perturbing compound that should be used with caution because it results in toxicity in many cell-based screens. [39] Moreover, MMV666023, which contains an azo group, produces toxic metabolites [37], indicating that it might not be suitable for human treatment.

Interestingly, MMV665881 and MMV085471 were predicted to interact with the same two immunodominant epitopes in the RBD: CoV2_S-10 (Pro412 and Lys417) and CoV2_S-11.2 (Lys462, Glu465, Arg466, and Tyr473). This may be the result of their high structural similarities. However, given that they only interact with epitopes within the RBD, the inhibitory effect of MMV665881 and MMV085471 against new SARS-CoV-2 variants may be decreased. This is because the residues in their target epitopes (CoV2_S-10 or CoV2_S-11.2) are the sites of amino acid changes in new variants, including the most recent omicron BA.5, which contains the amino acid substitutions D405A, R408S, K417N, S477N, and T478K. [40] In addition to MMV011895 and MMV007384, MMV019881 showed a high binding affinity for various epitopes of the spike protein; thus, it is also a noteworthy candidate as a SARS-CoV-2 inhibitor, despite the requirement for further investigation.

Because of its high mutation rate, at least 12 novel SARS-CoV-2 variants have been identified globally. The most recently reported variant is omicron, with increased transmissibility and reduced susceptibility to neutralization by some monoclonal antibody treatments and postvaccination sera. [2] In addition to the mutations within the RBD region, the omicron variant also bears amino acid changes within the NTD, including A67V and del69 - 70 within CoV2_S-2 and del143-145 and G142D within CoV2_S-3. [41] Interestingly, while the cytoplasmic tail of the SARS-CoV-2 spike protein plays a crucial role in the surface expression, intracellular trafficking, and membrane localization of the S protein, and syncytia formation when interacting with the ACE2 receptor [42], no amino acid change in this region of the omicron variant is reported. According to the binding affinity test of malaria box compounds regarding non-RBD epitope peptides, the selected compounds showed moderate-to-high interaction with both the NTD and cytoplasmic tail regions. With the potential of the selected epitopes to act as allosteric sites, the interaction between the tested malaria box compounds and residues in the non-RBD epitopes may affect the conformational change process of the SARS-CoV-2 spike protein and lead to the reduction or absence of trafficking signals during SARS-CoV-2 infection.

Altogether, our results provide information on potential candidates among MMV malaria box compounds, which are identified as antimalarial drugs, for SARS-CoV-2 inhibition by employing *in silico* molecular docking to identify compounds with high binding affinity to 12 SARS-CoV-2 epitopes, followed by ELISA and SPR assays to validate these interactions, which generate preliminary data on the binding affinity of the selected compounds to 12 SARS-CoV-2 epitopes and lay the groundwork for further optimization and in-depth studies. MMV665881 and MMV665943 had a high inhibitory effect on the RBD-ACE2 interaction, indicating their potential to be used in COVID-19 treatment. However, the inhibitory effects were observed at relatively high concentrations (100 μM), which may not be practical for therapeutic use because of potential toxicity and side effects. Further optimization to lower effective concentrations is necessary to obtain better therapeutic efficacy. Moreover, because of the high concentration and limited amount of compounds available in the study, the IC_{50} values of the compounds were not determined and need to be addressed in future research. Based on the SPR assay, several compounds exhibited the ability to bind to the B-cell epitopes in the non-RBD region. However, further experimental validation *in vitro* and *in vivo* is needed.

Conclusion

In silico molecular docking has identified malaria box compounds that showed high binding affinity to SARS-CoV-2 spike protein B-cell epitope. Of the 400 compounds, 20 (3 top scoring compounds/epitope) exhibited high binding affinity with their respective epitopes. Among them, four compounds could bind to two epitopes and three could bind to more than four epitopes, including MMV007384, MMV011895, and MMV019881, suggesting their potential to have increased inhibitory effect against SARS-CoV-2 when compared with other compounds that interact with one epitope.

MMV665881 and MMV665943 have exhibited significant inhibitory effects on the interaction between the RBD and ACE2. This suggests their potential activities to bind to SARS-CoV-2 spike protein and possible interference with the viral infection process, which could be beneficial for COVID-19 treatment. In addition, several compounds showed promising interactions with non-RBD epitopes, broadening the scope of potential therapeutic usage and application.

Acknowledgements

This study is supported by Kasetsart University Research and Development Institute and International SciKU Branding (ISB), Faculty of Science, Kasetsart University. Sangvansindhu C.'s PhD study is funded by the Science Achievement Scholarship of Thailand (SAST). We thank Nguitragool W. from the Department of Molecular Tropical Medicine and Genetics, Faculty of Tropical Medicine, Mahidol University, Thailand, for providing the malaria box compounds.

Conflicts of interest statement

All authors have completed and submitted the International Committee of Medical Journal Editors Uniform Disclosure Form for Potential Conflicts of Interest. None of the authors disclose any conflict of interest.

Data sharing statement

All data generated or analyzed during the present study are included in this published article. Further details are available for noncommercial purposes from the corresponding author on reasonable request.

References

1. Stróż S, Kosiorek P, Stasiak-Barmuta A. The COVID-19 inflammation and high mortality mechanism trigger. Immunogenetics 2024;76:15-25.
2. Parra-Lucares A, Segura P, Rojas V, Pumarino C, Saint-Pierre G, Toro L. Emergence of SARS-CoV-2 Variants in the world: How could this happen?. Life (Basel) 2022; 12:194.
3. Wu F, Zhao S, Yu B, Chen YM, Wang W, Song ZG, et al. A new coronavirus associated with human respiratory disease in China. Nature 2020;579:265-69.
4. Malik YA. Properties of coronavirus and SARS-Co V-2. Malays J Pathol 2020;42:3-11.
5. Chen Y, Guo Y, Pan Y, Zhao ZJ. Structure analysis of the receptor binding of 2019-nCoV. Biochem Biophys Res Commun 2020;525:135-40.
6. Lan J, Ge J, Yu J, Shan S, Zhou H, Fan S, et al. Structure of the SARS-CoV-2 spike receptor-binding domain bound to the ACE2 receptor. Nature 2020;581:215-20.
7. Peter EK, Schug A. The inhibitory effect of a coronavirus spike protein fragment with ACE2. Biophys J 2021;119:1001-10.
8. Wu C, Liu Y, Yang Y, Zhang P, Zhong W, Wang Y, et al. Analysis of therapeutic targets for SARS-CoV-2 and discovery of potential drugs by computational methods. Acta Pharm Sin B 2020;10:766-88.
9. Lim HX, Masomian M, Khalid K, Kumar AU, MacAry PA, Poh CL. Identification of B-Cell epitopes for eliciting neutralizing antibodies against the SARS-CoV-2 spike protein through bioinformatics and monoclonal antibody targeting. Int J Mol Sci 2022;23:4341.
10. Polyiam K, Phoolcharoen W, Butkhot N, Srisaowakarn C, Thitithanyanont A, Auewarakul P, et al. Immunodominant linear B cell epitopes in the spike and membrane proteins of SARS-CoV-2 identified by immunoinformatics prediction and immunoassay. Sci Rep 2021;11: 20383.
11. Boehm E, Kronig I, Neher RA, Eckerle I, Vetter P, Kaiser L. Novel SARS-CoV-2 variants: the pandemics within the pandemic. Clin Microbiol Infect 2021;27:1109-17.
12. Feng B, Fu K. Latest development of approved COVID-19 drugs and COVID-19 drugs undergoing late stage clinical trials. Front. Drug Discov 2023;3:1304129.
13. Thiruchelvam K, Kow CS, Hadi MA, Hasan SS. The use of remdesivir for the management of patients with moderate-to-severe COVID-19: a systematic review. Expert Rev Anti Infect Ther 2022;20:211-29.
14. Lewnard JA, McLaughlin JM, Malden D, Hong V, Puzniak L, Ackerson BK, et al. Effectiveness of nirmatrelvir-ritonavir in preventing hospital admissions and deaths in People with COVID-19: a cohort study in a large US health-care system. Lancet Infect Dis 2023;23:806-15.
15. Trøseid M, Arribas JR, Assoumou L, Holten AR, Poissy J, Terziã V, et al. Efficacy and safety of baricitinib in hospitalized adults with severe or critical COVID-19 (Bari-SolidAct): a randomised, double-blind, placebo-controlled phase 3 trial. Crit Care 2023;27:9.
16. Rosas IO, Bräu N, Waters M, Go RC, Hunter BD, Bhagani S, et al. Tocilizumab in hospitalized patients with severe Covid-19 Pneumonia. N Engl J Med 2021; 384:1503-16.
17. Parvathaneni V, Kulkarni NS, Muth A, Gupta V. Drug repurposing: a promising tool to accelerate the drug discovery process. Drug Discov Today 2019;24: 2076-85.
18. Pruijssers AJ, George AS, Schäfer A, Leist SR, Gralinksi LE, Dinnon KH 3rd, et al. Remdesivir inhibits SARS-CoV-2 in human lung cells and chimeric SARS-CoV expressing the SARS-CoV-2 RNA Polymerase in mice. Cell Rep 2020;32:107940.

19. Ansems K, Grundeis F, Dahms K, Mikolajewska A, Thieme V, Piechotta V, et al. Remdesivir for the treatment of COVID-19. Cochrane Database Syst Rev 2023;1:CD014962.
20. Hashemian SMR, Sheida A, Taghizadieh M, Memar MY, Hamblin MR, Bannazadeh Baghi H, et al. Paxlovid (Nirmatrelvir/Ritonavir): A new approach to Covid-19 therapy? Biomed Pharmacother 2023;162:114367.
21. Zhang X, Zhang Y, Qiao W, Zhang J, Qi Z. Baricitinib, a drug with potential effect to prevent SARS-COV-2 from entering target cells and control cytokine storm induced by COVID-19. Int Immunopharmacol 2020;86:106749.
22. Raiteri A, Piscaglia F, Granito A, Tovoli F. Tocilizumab: From Rheumatic Diseases to COVID-19. Curr Pharm Des 2021;27:1597-607.
23. Barnette KG, Gordon MS, Rodriguez D, Bird TG, Skolnick A, Schnaus M, et al. Oral sabizabulin for high-risk, hospitalized adults with Covid-19: Interim analysis. NEJM Evid 2022;1:EVIDoa2200145.
24. Noreen S, Maqbool I, Madni A. Dexamethasone: Therapeutic potential, risks, and future projection during COVID-19 pandemic. Eur J Pharmacol 2021;894:173854.
25. Gendrot M, Andreani J, Boxberger M, Jardot P, Fonta I, Le Bideau M, et al. Antimalarial drugs inhibit the replication of SARS-CoV-2: An in vitro evaluation. Travel Med Infect Dis 2020;37:101873.
26. Mahévas M, Tran VT, Roumier M, Chabrol A, Paule R, Guillaud C, et al. No evidence of clinical efficacy of hydroxychloroquine in patients hospitalised for COVID-19 infection and requiring oxygen: Results of a study using routinely collected data to emulate a target trial. medRxiv 2020;20060699.
27. Lamiable A, Thévenet P, Rey J, Vavrusa M, Derreumaux P, Tufféry P. PEP-FOLD3: Faster de novo structure prediction for linear peptides in solution and in complex. Nucleic Acids Res 2016;44(W1):W449-W54.
28. Shen Y, Maupetit J, Derreumaux P, Tufféry P. Improved PEP-FOLD approach for peptide and miniprotein structure prediction. J Chem Theory Comput 2014;10: 4745-58.
29. Thévenet P, Shen Y, Maupetit J, Guyon F, Derreumaux P, Tufféry P. PEP-FOLD: an updated de novo structure prediction server for both linear and disulfide bonded cyclic peptides. Nucleic Acids Res 2012;40(Web Server issue):W288-93.
30. Hsu KC, Chen YF, Lin SR, Yang JM. iGEMDOCK: a graphical environment of enhancing GEMDOCK using pharmacological interactions and post-screening analysis. BMC Bioinformatics 2011;12 Suppl 1(Suppl 1):S33.
31. Fong KY, Sandlin RD, Wright DW. Identification of â-hematin inhibitors in the MMV Malaria Box. Int J Parasitol Drugs Drug Resist 2015;5:84-91.
32. Lucantoni L, Duffy S, Adjalley SH, Fidock DA, Avery VM. Identification of MMV Malaria Box inhibitors of Plasmodium falciparum early-stage gametocytes using a luciferase-based high-throughput assay. Antimicrob Agents Chemother 2013;57:6050-62.
33. Duffy S, Avery VM. Identification of inhibitors of Plasmodium falciparum gametocyte development. Malar J 2013;12:408.
34. Sun W, Tanaka TQ, Magle CT, Huang W, Southall N, Huang R, et al. Chemical signatures and new drug targets for gametocytocidal drug development. Sci Rep 2014;4:3743.
35. Bowman JD, Merino EF, Brooks CF, Striepen B, Carlier PR, Cassera MB. Antiapicoplast and gametocytocidal screening to identify the mechanisms of action of compounds within the malaria box. Antimicrob Agents Chemother 2014;58:811-9.
36. Linares M, Viera S, Crespo B, Franco V, Gómez-Lorenzo MG, Jiménez-Díaz MB, et al. Identifying rapidly parasiticidal anti-malarial drugs using a simple and reliable in vitro parasite viability fast assay. Malar J 2015;14:441.
37. Paiardini A, Bamert RS, Kannan-Sivaraman K, Drinkwater N, Mistry SN, Scammells PJ, et al. Screening the medicines for malaria venture "Malaria Box" against the Plasmodium falciparum aminopeptidases, M1, M17 and M18. PloS One 2015;10:e0115859.
38. von Koschitzky I, Gerhardt H, Lämmerhofer M, Kohout M, Gehringer M, Laufer S, et al. New insights into novel inhibitors against deoxyhypusine hydroxylase from plasmodium falciparum: compounds with an iron chelating potential. Amino Acids 2015;47:1155-66.
39. Ramsey NB, Andersen OS. Bilayer effects of antimalarial compounds. PloS One 2015;10:e0142401.
40. Chatterjee S, Bhattacharya M, Nag S, Dhama K, Chakraborty C. A detailed overview of SARS-CoV-2 omicron: Its sub-variants, mutations and pathophysiology, clinical characteristics, immunological landscape, immune escape, and therapies. Viruses 2023; 15:167.
41. Wu L, Zhou L, Mo M, Liu T, Wu C, Gong C, et al. SARS-CoV-2 Omicron RBD shows weaker binding affinity than the currently dominant Delta variant to human ACE2. Signal Transduct Target Ther 2022;7:8.
42. Cattin-Ortolá J, Welch LG, Maslen SL, Papa G, James LC, Munro S. Sequences in the cytoplasmic tail of SARS-CoV-2 spike facilitate expression at the cell surface and syncytia formation. Nat Commun 2021;12:5333.